STRESS AND STRAIN IN FRONT OF THE FATIGUE CRACK WITH SHEAR LIPS

A. Materna and V. Oliva
Department of Materials, Faculty of Nuclear Sciences and Physical Engineering,
Czech Technical University in Prague, Czech Republic

ABSTRACT

Fatigue crack with curved front and shear lips in Al-alloy sheet was modelled using three-dimensional boundary and finite element methods. Local fracture mechanics parameters (stress intensity factor and energy release rate) together with parameters of stress–plastic strain field ahead of the crack front (normal and shear stresses in the local crack plane, maximum shear stress, plastic strain energy density and plastic zone size) are computed. It is shown that both local stress intensity factor range and energy release rate distributions do not correspond to the experimentally observed crack growth rate along the front. In addition, common criteria for mixed-mode propagation fail to predict the slanted crack growth direction. Focusing on the stress state, tensile mode could be characterized by very high normal stresses whereas shear stresses in the crack plane are negligible. In the shear mode, high shear stresses in the crack plane act together with some normal stress. Moreover, there is a larger plastic zone around the whole shear lip and, therefore, large plastic strain energy density dissipated ahead of the slant crack front. Plasticity induced closure is very intensive in the relatively thin surface layer.

1 INTRODUCTION

The present authors have recently studied deformation mechanics around the propagating through-thickness planar fatigue crack with straight (Oliva [1]) and realistically curved front (Oliva [2]). The primary motivation of such FEM computations was an extension of usual two-dimensional fracture mechanics concepts for cracks under loading mode I to three dimensions. A quantitative understanding of three-dimensional effects could improve the methodology for the fatigue crack growth rate prediction in more complicated crack configurations (e.g., surface cracks and through-thickness cracks in parts with complex cross-sectional area). Some attention has also been paid to direct evaluation of the crack growth rate from parameters of the stress and strain field around the crack front. Such approaches based mostly on HRR estimation of the energy dissipated ahead of the crack front have recently appeared more frequently (e.g., Skelton [3], Pandey [4]).

In this paper, numerical simulation of the cyclic stress-strain field in front of the fatigue crack with shear lips is discussed. The model curved crack front shape is chosen to closely correspond to the crack front obtained experimentally. The model presented represents a new approximation of the real fatigue crack.

2 STARTING EXPERIMENT

Measurements of the fatigue crack growth in CCT specimen (180×58×6mm) from Al-alloy 2024 T-42 were performed in the Aeronautical Research and Testing Institute in Prague (Balasova [5]). The loading was periodic with stress range $\Delta S = 44.96$ MPa and stress ratio $R = 0$.

When the crack reached a surface length of 6.525 mm, shear lips started to form. Since that moment, the middle part of the crack has remained planar, whereas the marginal part has been growing in a slanted plane at an observed angle of about 63° from the flat crack plane.

The surface length of the simulated crack is 9.098 mm. The corresponding crack front shape was determined optically from fracture surface, and it can be described as follows: the crack

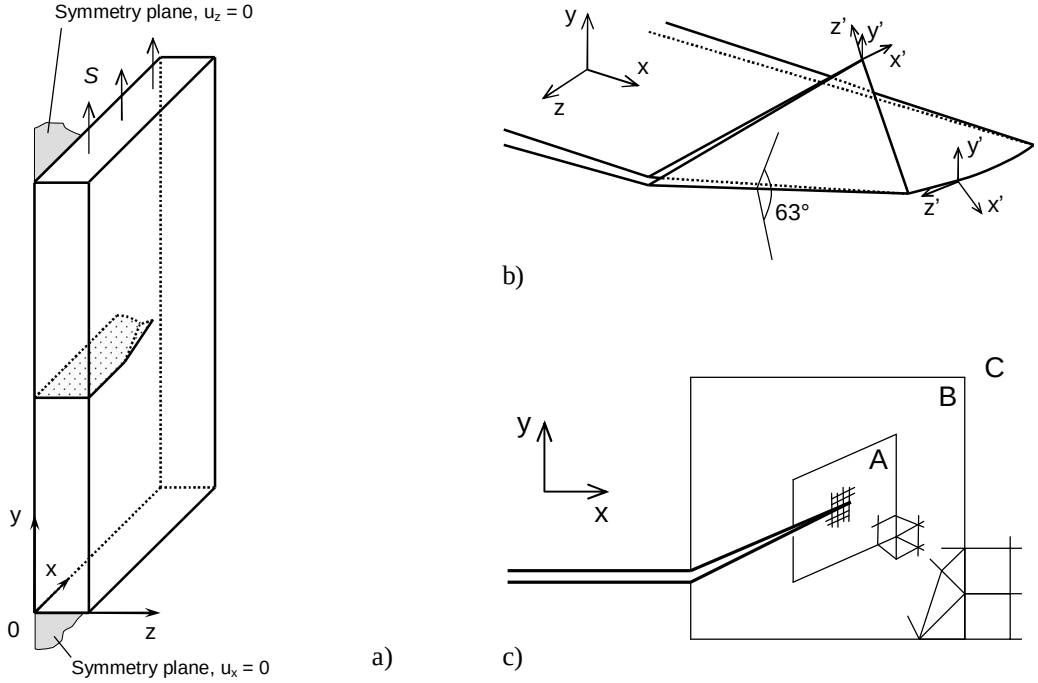

Figure 1: Geometry and model of the CCT specimen:
a) Specimen geometry with model boundary conditions.
b) Crack surface geometry.
c) Schematic of finite element mesh construction.

front in the tensile mode area exhibits typical tunnelling with a depth of approximately 0.6 mm; the crack front in slanted plane is straight and perpendicular to the global growth direction.

3 NUMERICAL MODEL

3D nonlinear finite element model was created using software MSC.Marc. Fig. 1a is schematic of the modelled part of the specimen and the global coordinate system x, y, z. There is no symmetry condition in xz plane. Therefore, one quarter of the specimen had to be modelled, and symmetrical constraints were added to simulate the rest of the body.

Because of 3D shape of the crack front, the finite element mesh construction was complicated. The resulting mesh consists of three connected parts A, B, and C (see Fig. 1c). 8-noded hexahedral elements in A were created by expansion of quadrilateral elements along the curved front. The element size varies – the smallest elements 2×2×2μm are situated at the front under the free surface, where large stress and strain gradients were expected. The element size increases towards the centre of the thickness and away from the crack front. The number of elements along the slant and flat part of the front is 11 and 9, respectively. Four-noded tetrahedral elements in the transition part B were produced by automatic generator. The rest of body C is covered by a regular mesh consisting of 8-noded hexahedral elements. Each boundary element from A and C is connected to two boundary elements from B.

The material behaviour was considered as elastic-plastic with kinematic hardening. Small strain formulation was used.

In order to prevent the crack surfaces from penetrating, contact algorithm had to be used. The relative motion of crack surfaces is tracked, and when contact occurs, direct constraints are placed on the motion using boundary conditions – both kinematic constraints on transformed degrees of freedom and nodal forces [6]. Crack advance is realized by the change of contact algorithm parameters: relative motion between unfractured (future) crack surfaces is not permitted. A prescribed front jump is modelled by enabling relative motion between elements adjacent to the crack plane ahead of the crack front during the so-called active cycles. An "idle" model cycle without crack propagation is inserted between two active cycles. It is reasonable to suppose that the crack front deformation mechanics in the idle cycle will be close to that in the real cycle with very small crack extension. The total prescribed crack extension during 44 applied model load cycles was 0.45 mm. In the simulation presented, no friction of crack surfaces was involved.

The distribution of the local stress intensity factors along the 3D crack front was computed using boundary element method implemented in the program FRANC3D/BES (http://www.cfg.cornell.edu).

4 DISCUSSION

4.1 *Fracture mechanics approach*

In Fig. 2, elastic stress intensity factor ranges for three loading modes are plotted vs. the distance from mid-thickness. For comparison, also ΔK_I in a hypothetical case, when shear lips formation would be suppressed, is plotted. The crack front curvature near the free surface was supposed to be the same as observed for a little shorter flat crack. As shown, the rise of shear lips substantially changes the local fracture mechanics parameters along the crack front. ΔK_I increases from the middle towards the specimen surface because of crack tunnelling. Near the transition from flat to slant type of growth (transition point), the increase of ΔK_I is even more intensive compared to the case without shear lips. Nevertheless, behind the transition point, ΔK_I falls to the half of the previous value and gradually decreases towards the free surface.

It is generally assumed that shear lips grow mainly under combined mode I and III. The value of ΔK_{III} in slant part is really high and it only slightly decreases towards the specimen surface. Surprisingly, the absolute value of ΔK_{II} near the surface is comparable with ΔK_{III}. Nonzero values of ΔK_{II} and ΔK_{III} are induced already in the flat part of the crack near the transition point, which could support the subsequent increase in shear lip width.

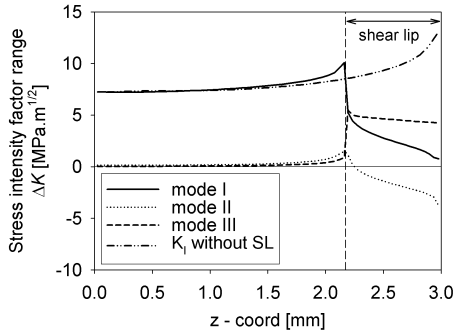

Figure 2: Stress intensity factors distributions along the front of the crack with and without shear lips

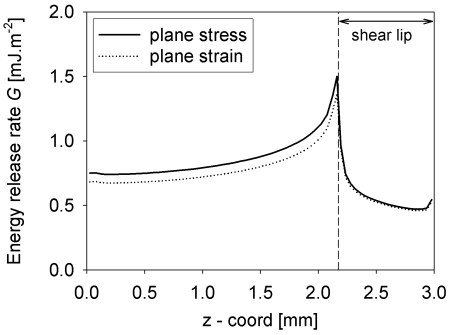

Figure 3: Energy release rate distribution along the front of the crack with shear lips

To involve an effect of all crack modes into one parameter, the energy release rate according to formula

$$G = \frac{K_I^2}{E'} + \frac{K_{II}^2}{E'} + \frac{1+\nu}{E} K_{III}^2 \tag{1}$$

can be evaluated. $E' = E$ and $E' = E/(1-\nu^2)$ are elastic constants for plane stress and plane strain, respectively. In the flat crack region, where plane stress and plane strain solutions differ, plane strain is reasonably the proper one. Displayed non-uniform dependence in Fig. 3 is in contrast to an experimental fact that the local crack growth rate is roughly constant along the whole front.

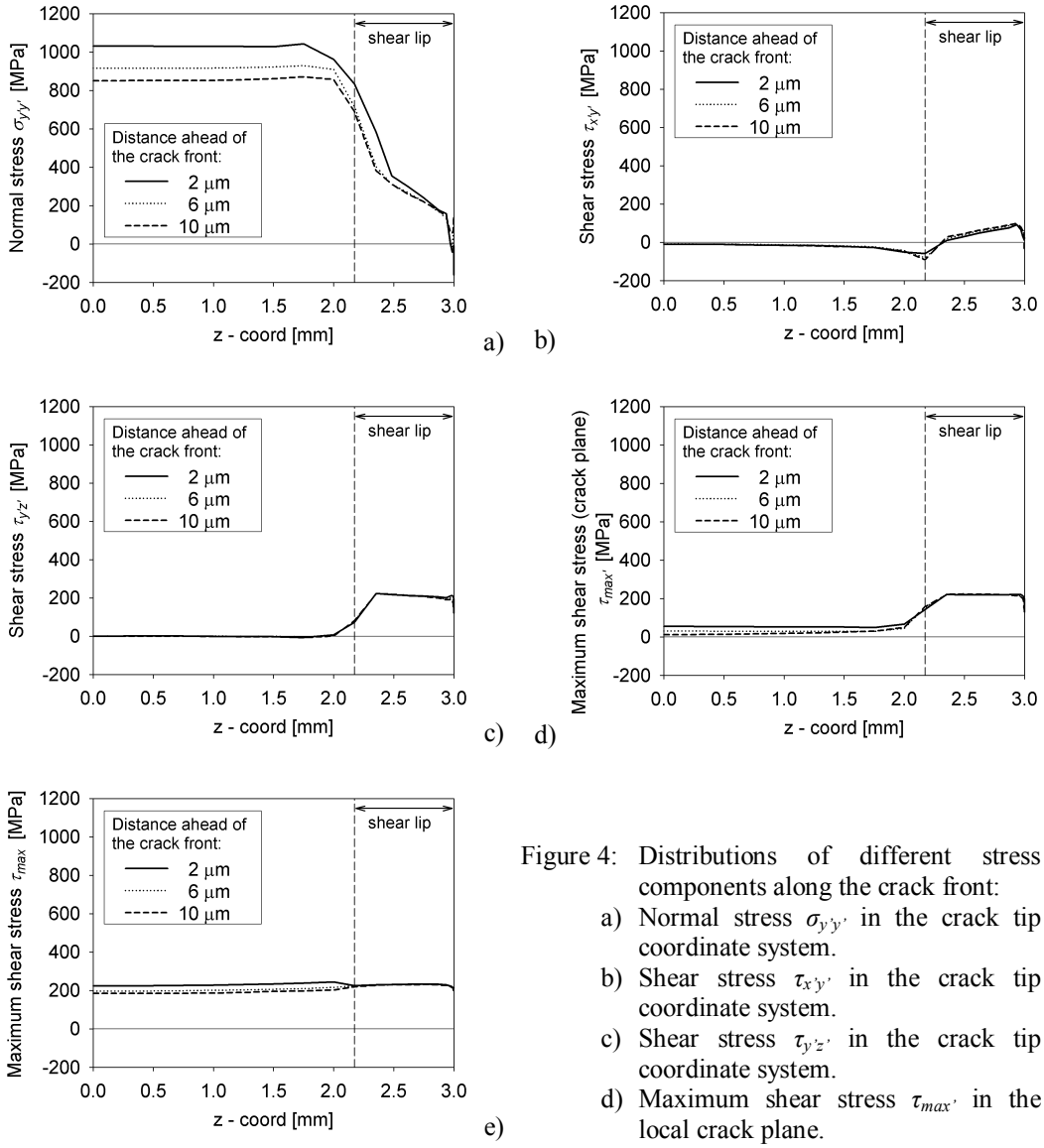

Figure 4: Distributions of different stress components along the crack front:
a) Normal stress $\sigma_{y'y'}$ in the crack tip coordinate system.
b) Shear stress $\tau_{x'y'}$ in the crack tip coordinate system.
c) Shear stress $\tau_{y'z'}$ in the crack tip coordinate system.
d) Maximum shear stress $\tau_{max'}$ in the local crack plane.
e) Overall maximum shear stress τ_{max}.

4.2 *Cyclic stress and plastic strain along the crack front*

A possible mechanical concept of the crack propagation under remote mode I cyclic loading is quite simple and serves also as a basis for, e.g., dislocation models (Deshpande [7]): Crack growth can be driven by shear stress in the planes of high shear which produces dislocation slip, and by tensile stress normal to the crack plane which leads to final cohesive separation of damaged material. This concept is in agreement with the results achieved ahead of the crack front in tensile mode. The crack propagates in a plane with practically zero shear and maximum normal stresses.

A similar concept for shear mode propagation is not clear. Numerical simulation in the shear lips area indicates that the experimentally observed plane of propagation is not given by the maximum tangential stress condition and it is slightly inclined also to the plane of maximum shear stress. An open question therefore is: in which planes does slip occur and which of the stresses acting in the crack plane control the final fracturing (normal, shear, or both)? To compare material loading ahead of the flat and slant part of the crack, a local coordinate system x'y'z' was defined. x' axis is perpendicular to the front, y' is perpendicular to the crack plane, and z' is in tangential direction (Fig. 1b).

Distributions of stresses $\sigma_{y'y'}$, $\tau_{x'y'}$, $\tau_{y'z'}$ along the crack front are plotted in Figs. 4a, 4b, 4c. They roughly correspond to SIF distributions ΔK_{I}, ΔK_{II}, and ΔK_{III} displayed in Fig. 2. The maximum shear stress τ_{max}' in the crack plane x'z' is shown in Fig. 4d. The difference between both fracturing modes is evident from comparison of Fig. 4a and 4d. The decrease of normal stress and reciprocal increase of shear stress in the crack plane seems to be typical of shear mode. Normal and shear stresses are present along the whole shear lip (see Fig. 4a, d).

Contrary to τ_{max}', the absolute maximum shear stress τ_{max} is due to the presence of plastic deformation practically constant along the crack front (Fig. 4e). Only planes of maximum shear stress are different. Ahead of slant crack front, τ_{max} is close to τ_{max}' (compare Figs. 4d and 4e), and its value is given mainly by value of the stress component $\tau_{y'z'}$ (compare Figs. 4b, 4c and 4e).

Fig. 5 shows the plastic zone size in plane x'z', determined according to the condition of nonzero equivalent plastic strains. The extensive zone detected along the whole slant crack front is not localized only into the thin surface layer, as in the case of planar crack with curved front (Oliva [2]).

The plastic zone size corresponds to the distribution of plastic strain energy density dissipated ahead of the crack front (Fig. 6). Both dissipated energy and critical energy to fracture are several times higher for the shear mode than for the tensile mode.

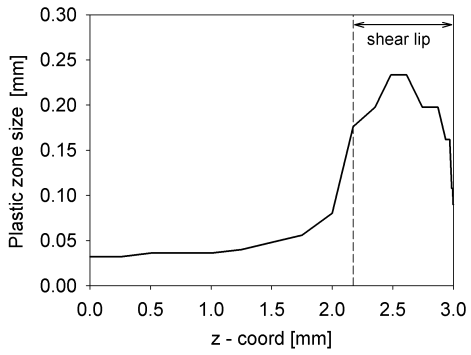

Figure 5: Plastic zone size along the crack front

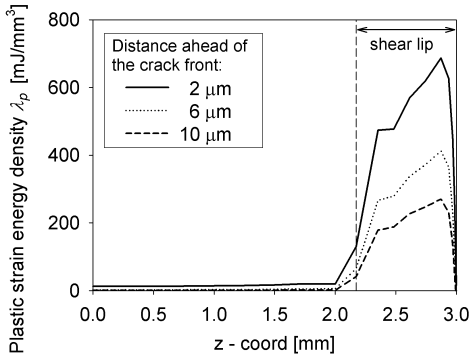

Figure 6: Plastic strain energy density along the crack front

A quantitative characterization of plasticity induced crack closure is essential for an assessment of effective values of stress intensity factors. At this moment, the results achieved provide only a basic qualitative view: no plasticity-induced closure appears in the mid-thickness, whereas the closure is very intensive in the surface layer.

4 CONCLUSIONS

A 3D numerical simulation of the growing fatigue crack with shear lips supports the following conclusions:

1. All the three loading modes are present in slant growth. Maxima of ΔK_{I}, ΔK_{II}, and ΔK_{III} occur in different positions at the crack front, but are comparable in their absolute values.
2. Common criteria for prediction of the mixed-mode crack propagation direction fail for the shear lips area.
3. Detailed fracture mechanics interpretation of the simulation is full of difficulties because there are no reliable parameters describing the fatigue crack behaviour in shear lip area.
4. In tensile mode, very high normal stresses and negligible shear stresses act in the crack plane. In shear mode, high shear stresses in the crack plane act together with some normal stresses.
5. Both plastic zone size and plastic strain energy density dissipated ahead of the crack front are several times higher for the shear mode than those for the tensile mode.
6. In the mid-thickness, no plasticity-induced closure appears, whereas in the surface layer the closure is very intensive.

Financial support for this research by the Grant Agency of the Czech Republic, through grant No. 101/03/0331 "FEM Simulations of Fatigue Crack Propagation under Complex Service Conditions" is gratefully acknowledged.

REFERENCES

[1] Oliva, V. – Materna, A. – Michlik, P.: Three-Dimensional FEM Model of the Fatigue Crack Growth in a Thick CT Specimen, In: Proceedings of the 3rd International Conference on Materials Structure & Micromechanics of Fracture, pp. 368-378, 2001

[2] Oliva, V. – Materna, A. – Denk, T.: FEM Model of Planar Fatigue Crack with Curved Crack Front, In: Fractography 2003, IMR SAS Kosice, pp. 26-33, 2003

[3] Skelton, R.P. – Vilhelmsen, T. – Webster, G.A.: Energy criteria and cumulative damage during fatigue crack growth, Int. J. Fatigue, 20, pp. 641-649, 1998

[4] Pandey, K.N. – Chand, S.: An energy based fatigue crack growth model, Int. J. Fatigue, 25, pp. 771-778, 2003

[5] Balasova, M. – Berankova, I. – Panek, M.: Characterization of fatigue crack growth in 6mm thick MT-specimens made from aeronautical material 2024-T42, Report Z-3669/98, VZLU Praha-Letnany, 1988 (in czech)

[6] MSC.Marc Volume A – Theory and User Information, 2003

[7] Deshpande, V.S. – Needleman, A. – Van der Giessen, E.: Discrete dislocation modeling of fatigue crack propagation, Acta Materialia, 50, pp. 831-846, 2002